A Hamiltonian graph model for cooperative toughening of crystalline phases and covalent adaptable networks in semi-crystalline thermoset epoxy

Jing Zhang[1], Haibao Lu[1,3], Ahmed Elmarakbi[2] and Yong-Qing Fu[2,3]

[1]National Key Laboratory of Science and Technology on Advanced Composites in Special Environments, Harbin Institute of Technology, Harbin, 150080, PR China

[2]Faculty of Engineering and Environment, University of Northumbria, Newcastle upon Tyne, NE1 8ST, UK

[3]Corresponding author HBL: luhb@hit.edu.cn, YQF: richard.fu@northumbria.ac.uk

Abstract: Attributed to its existence of bond exchange reactions (BERs) and covalent adaptable networks (CANs), thermoset epoxy has shown self-healing and reversibly mechanical capabilities. However, toughening mechanisms and cooperative coupling of these crystal phases and CANs in a semi-crystalline thermoset epoxy have not been well understood. In this study, a Hamiltonian graph model is formulated to explore toughening mechanisms in the semi-crystalline thermoset epoxy based on the vertices and paths, both of which are employed to describe the crystalline phases and CANs, respectively. A free-energy equation is further developed based on the tail and tie free energy functions to investigate the cooperative coupling of crystal phases and CANs. The crystal phases increase the cross-linking density of the CANs, which help the crystal phases with a homogeneous dispersion. Moreover, an extended Maxwell model is developed along with the Hamiltonian graph to explore the coupling effect of crystal phases and CANs on the mechanical behaviors of semi-crystalline thermoset epoxy. A constitutive stress-strain relationship is then proposed to describe

the self-healing and toughening behaviors of semi-crystalline thermoset epoxy. The stress-strain relationship of semi-crystalline polymers, which incorporates the crystal phases and CANs, has been thoroughly investigated using the analytical results obtained from the proposed Hamiltonian graph model. Finally, effectiveness of the proposed model is verified using the finite element analysis and a set of experimental data.

Keywords: epoxy, covalent adaptable network, crystal, Hamiltonian graph

1. Introduction

Covalent adaptable networks (CANs), which are incorporated of reversible covalent bonds undergoing bond exchange reactions (BERs), enable thermoset epoxy polymers with good capabilities of self-healing [1-3], reprocessing [4,5] and recycling [6,7]. Experimental results revealed that the epoxy polymers with CANs can achieve excellently reversible mechanical properties [8,9], thus having great practical applications in the fields such as aerospace [10,11], manufacturing industry [12,13] and 3D printing [14,15].

Although many experimental and theoretical studies have been conducted to produce or predict the thermoset epoxy with self-healing and interfacial welding properties based on the designs of CANs using the BERs [16-20]. Currently, mechanochemistry relationships between their dynamic covalent bonds and mechanical behaviors have not been well understood, mainly due to their complex cooperativity and coupling effects. Previously, Qi et.al used a multi-branched Maxwell model to investigate the mechanochemical coupling effect on the kinetic

relaxation time of CANs in a thermoset epoxy [16]. Yu et.al. proposed a framework model to investigate the scaling relationship between covalent bonds and macroscopic self-healing behaviors of the thermoset epoxy [17]. Shi et.al. developed a relaxation time model to predict interfacial welding behaviors of a thermoset epoxy undergoing the BERs [18]. Furthermore, topological entanglement models of CANs have been developed to describe toughening mechanisms of the epoxy polymer with the chemical BERs [18-20]. On the other hand, to improve tensile strength and maximum elongation at the breaking of the epoxy, various fillers have been added to reinforce the epoxy matrix [21-23]. Some crystalline phases were also applied to be homogeneously dispersed into the CANs, and the formed semi-crystalline epoxy showed excellent mechanical properties compared with those amorphous ones [24-26].

Finite element analysis (FEA) method has been played a crucial role for design and optimization of high-performance multiphase/multicomponent materials. Gohari et al [27] did simulation analysis and obtained the analytical solutions for multi-phase material mixed rectangular plate under the action of water and air. The analysis was also strengthened according to the wave form of the component materials [28]. FEA has also been successfully used to study the static and dynamic deformation responses of the multi-component materials [29].

Based on an extensive literature, we found that combination of crystal phases and CANs have resulted in the significant improvements of mechanical performance of the semi-crystalline thermoset epoxy [30]. However, its self-healing and toughening

mechanisms behind these phenomena have not been fully understood, and both the theoretical models and experimental studies are urgently needed. In this study, a Hamiltonian graph model is firstly formulated to explore the toughening mechanisms and cooperative coupling of crystal phases and CANs using vertices and Hamiltonian paths, both of which enhance the transfer capability for loads in the semi-crystalline thermoset epoxy. In this model, crystal phases are applied as the cross-linking points and vertices in the CANs. These modified CANs are then used to connect the crystal phases and provide the Hamiltonian paths for mechanical load transfer in the semi-crystalline epoxy. We prove that there is a cooperative coupling between crystal phases and CANs which influences the toughening behaviors of semi-crystalline thermoset epoxy. Based on the tail and tie free energy functions [31], a free-energy equation is also developed to explore the constitutive stress-strain relationship of semi-crystalline thermoset epoxy using the extended Maxwell model. Finally, effectiveness of the proposed model is verified using both the finite element analysis and experimental results.

2. Materials and mechanical testing

2.1 Material synthesis

The epoxy samples were synthesized using an epoxy monomer of diglycidyl-ether bisphenol A (DGEBA, Sigma Aldrich) and a cross-linker of glutaric anhydride. Two types of epoxy samples were prepared, e.g., amorphous epoxy and semi-crystalline epoxy. The stoichiometric ratios between the epoxy and glutaric anhydride were set as 1:0.5 and 1:1, respectively. Cross-linking agent was initially mixed with the DGEBA

in a beaker and stirred at 80°C for 45 min, and then the obtained mixture was left in an oven under a vacuum. The obtained mixture was poured into a mold and cured in the oven at 160°C for 24 hours for the full polymerization of epoxy polymers. The synthesized network contained ester bonds on the chain's backbone, which were participated in transesterification of BERs during the self-healing process of the epoxy. The DGEBA monomer was opened from both ends of its loop structure and was polymerized by the crosslinkers to form a chain.

The variations in the extents of curing reactions were identified using a Fourier transform infrared spectroscope (FTIR, Nicolet, Thermo-Fisher Scientific). The representative IR spectra of the epoxy and semi-crystalline epoxy specimens before and after curing are shown in Figure 1, the data of which were obtained by scanning the samples for 32 times in a range from 550 to 4000 cm^{-1} at a resolution of 1 cm^{-1}. The disappearance or formation of characteristic groups or bonds during the curing process was verified. The functional epoxy groups exhibited a characteristic absorption peak of ester at 1730 cm^{-1} [32], which was resulted from the cross-linking between epoxy and anhydride groups. Meanwhile, the curing reactions resulted in the shift of the band of epoxy group to 917 cm^{-1} in the FTIR spectra [33], due to the disappearance of epoxy groups after curing. Therefore, the epoxy and semi-crystalline epoxy were verified to be fully cured.

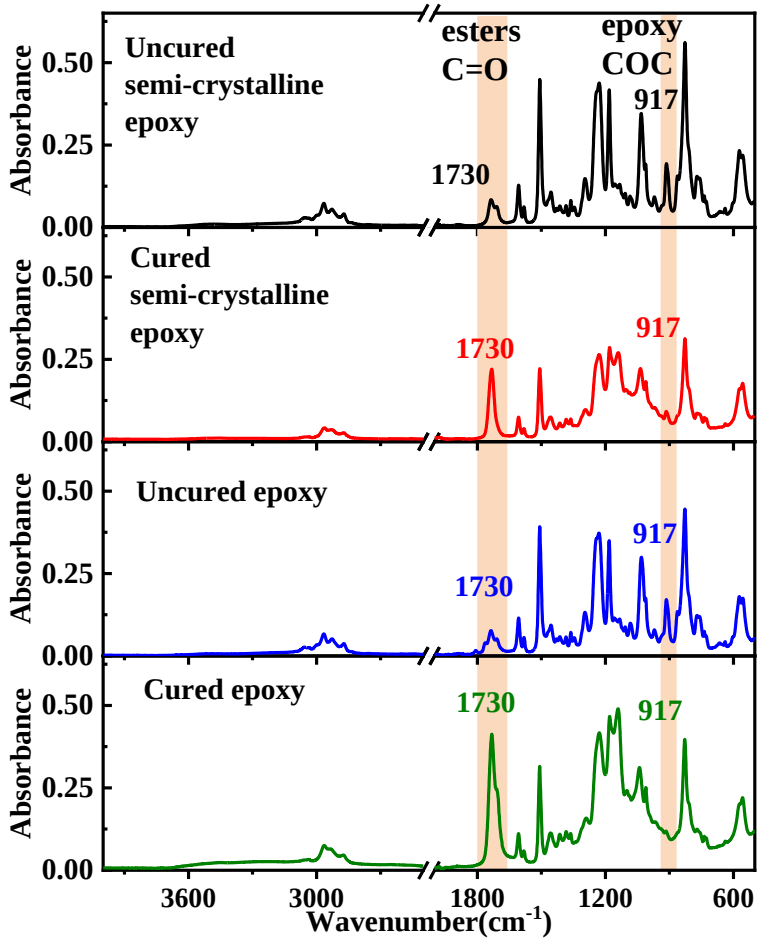

Figure 1. The representative FTIR spectra obtained from the uncured epoxy, cured epoxy, uncured semi-crystalline epoxy and cured semi-crystalline epoxy specimens.

2.2 Mechanical testing

The epoxy and semi-crystalline epoxy specimens with dimensions of 20×4×2 mm^3 were tested using to the Dynamic Mechanical Analysis (DMA, Model Q800, TA Instruments) for performing the dynamic bending under an isothermal heating process. The specimens were initially stabilized at 0 °C for 10 min, then heated from 0°C to 120°C at a heating rate of 2 °C/min. Figure 2 shows the DMA results, in which the semi-crystalline epoxy specimen presents a melting transition temperature at 25.16°C and a glass transition temperature at 79.53°C. On the other hand, the amorphous epoxy specimen only presents a glass transition temperature at 88.17°C.

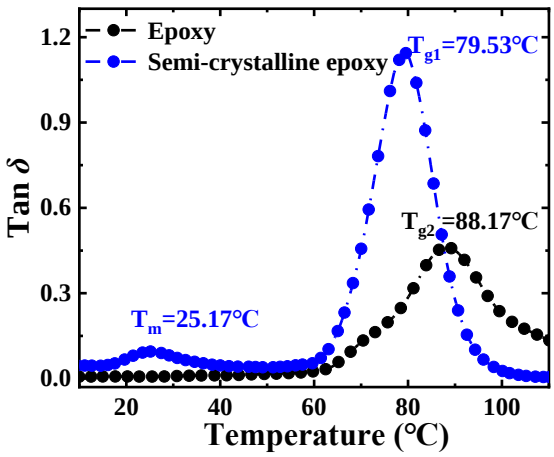

Figure 2. The glass transition temperature and melting transition temperature of epoxy and semi-crystalline epoxy specimens determined by the DMA measurements.

An electronic universal testing machine (AGXplus, Shimadzu) was used to evaluate the stress-strain behaviors of amorphous epoxy (epoxy1) and semi-crystalline epoxy (epoxy2), with a dimension of 100×10×2 mm^3. The specimens were tested at a strain rate of 0.00058 s^{-1} according to ASTM/D638. As shown in Figure 3(a), the tensile strength was decreased from 66.3 MPa of the semi-crystalline epoxy to 22.6 MPa of the amorphous epoxy. This is mainly due to the decrease in the content of cross-linking agent of glutaric anhydride in the semi-crystalline epoxy specimen, because the DGEBA promotes the formation of crystalline phases in the epoxy polymer [34], thus enhancing tensile strength. Based on the rubber elasticity theory, the increase of cross-linking degree of crystalline phases in the polymer network leads to an increase of tensile strength [35].

The BERs were then employed into the polymer network in epoxy. As shown in Figure 3(b), an increased tensile strength of 24.1 MPa was obtained for the epoxy specimen with adding the BERs, compared with 22.6 MPa for that of epoxy specimen without BERs. While the yielding strain was then decreased from 0.055 of epoxy

specimen with BERs to 0.03 of epoxy specimen without BERs.

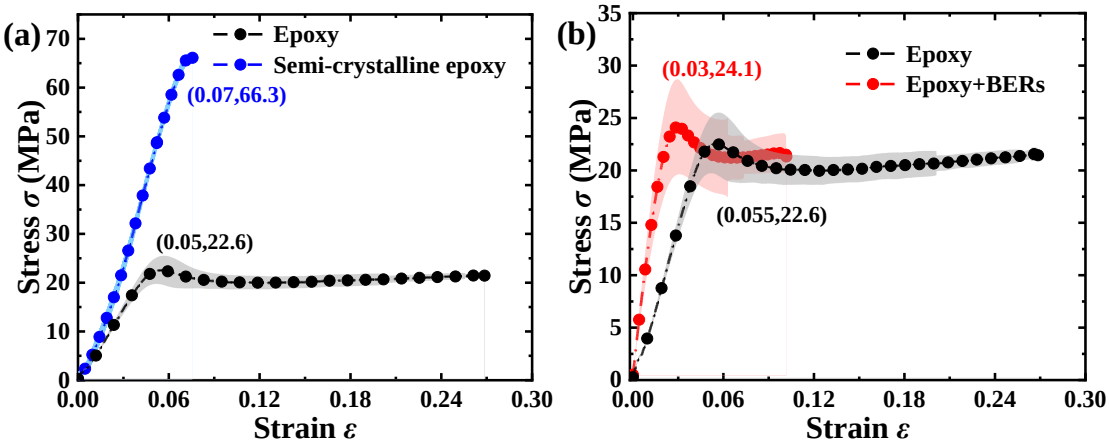

Figure 3. (a) Experimental stress-strain results of amorphous epoxy and semi-crystalline epoxy specimens. (b) Experimental stress-strain results of amorphous epoxy specimens with and without BERs.

3. Theoretical framework

3.1 An extended Maxwell model based on Hamilton graph

A semi-crystalline epoxy is commonly incorporated of two components, i.e., crystalline phase and CAN. As shown in Figure 4(a), there are two distinctly different Hamilton paths, which are needed to transfer the externally mechanical force. The crystalline phase and CAN can be treated as the vertex and side in the Hamilton graph model [36]. In comparison with that of CAN, the crystalline phase can provide a higher amount of vertexes, which enhance the Hamilton paths in the polymer networks of a semi-crystalline epoxy. Here the CAN is applied to achieve a homogeneous dispersion of crystalline phases, as shown in the Figure 4(b).

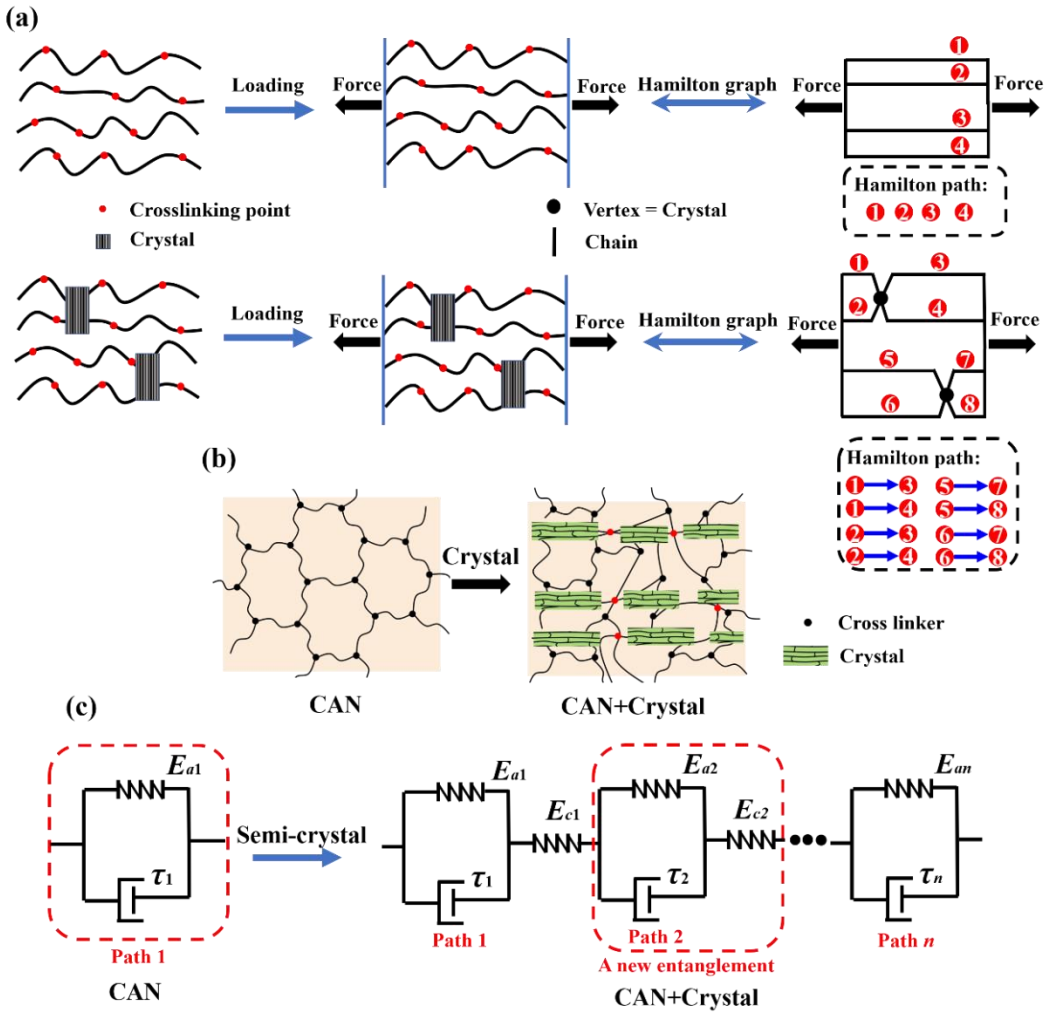

Figure 4. (a) Schematic illustrations of effects of CANs and crystalline phase on Hamilton paths in response to externally mechanical force. (b) CAN structure modified by the crystal phases. (c) Effect of Hamilton path on the Maxwell model in semi-crystalline epoxy.

An extended Maxwell model is then developed to describe the effect of crystalline phase on the viscoelastic modulus of the semi-crystalline epoxy. With an increase in the number of Hamilton paths, more viscoelastic branches have been involved to resist to the externally mechanical force according to the Maxwell model, and these viscoelastic branches can simultaneously enhance the strength of the semi-crystalline epoxy, as revealed in Figure 4(c).

3.2. Constitutive stress-strain relationship

According to the Hamilton graph model [36] and Maxwell model [37], a constitutive stress-strain relationship of epoxy polymer can be formulated,

$$\sigma = \sum_{i=1}^{n}\left(\Phi_{ci} E_{ci} \varepsilon + \Phi_{ai} E_{ai} \tau_i \dot{\varepsilon} \left[1 - \exp(-\frac{\varepsilon}{\tau_i \dot{\varepsilon}}) \right] \right) \quad (1)$$

where Φ_{ci} and E_{ci} are the fraction and modulus of the *i*th crystal phase, respectively, Φ_{ai} and E_{ai} are the fraction and modulus of the *i*th amorphous phase, respectively, τ is the relaxation time, ε is the strain, $\dot{\varepsilon}$ is strain rate, and $\varepsilon=\dot{\varepsilon}t$ in the strain.

Based on the rubber elasticity theory [38], the modulus of an amorphous phase (Ea) can be expressed as,

$$E_a = 3(N + N_t)RT \quad (2)$$

where N is the molar number of cross-linking chains, N_t is the molar number of entanglements between crystal phase and cross-linking chain, R=8.314 J/mol·K is the gas constant, and T is the temperature.

Based on the free volume theory [39], the diffusion coefficient (D_{co}) as a function of free volume can be expressed as,

$$D_{co} = D_0 \exp\left(-\frac{E_{as}}{RT} - \frac{\gamma}{(1 - k_{so}t)\Delta V} \right) \quad (3)$$

where D_0 is the referenced diffusion coefficient, E_{as} is the activation energy of diffusion, γ=0.5~1 is a given constant [39], ΔV is the change ratio in free volume, and k_{so} represents the volatilization coefficient.

Here the modulus is determined by both the diffusion coefficient and relaxation time, τ_s. In a semi-crystalline epoxy, there are two types of relaxation times, i.e., $\tau_s=\tau_b+\tau_c$, τ_b and τ_c represent the relaxation times for BER and diffusion, respectively.

The diffusion coefficient is related to its moving distance and diffusion time by $l_0^2 = D_{co}\tau_c$ [17]. Stukhalin et al. [40] proposed an expression for the relaxation time of BER (τ_b) as, □

$$\tau_b \approx \tau_0 \exp\left(\frac{E_{ab}}{RT} + \frac{\gamma}{(1-k_{so}t)\Delta V}\right) \tag{4}$$

$$N_t = \frac{N_{t0}t}{\tau_s} \tag{5}$$

where τ_0 is the reference of relaxation time, E_{ab} is the activation energy of BER, and N_{t0} is the molar number of reactive chain per unit volume.

Combining equations (2), (3), (4) and (5), the modulus of amorphous phase (E_a) can be obtained,

$$E_a = 3\left[N + \frac{tN_{t0}\exp\left(-\frac{\gamma}{(1-k_{so}t)\Delta V} - \frac{E_{ab}}{RT}\right)}{\tau_0 + \frac{l_0^2}{D_0}\exp\left(\frac{E_{as}-E_{ab}}{RT}\right)}\right]RT \tag{6}$$

On the other hand, the tail and tie free energy functions [31] can be employed to characterize the crystal phase as follows,

$$\frac{F_{tail}(\xi,m)}{k_BT} = \ln\left(\frac{\xi}{4\ell}\right) + \frac{2\pi^2}{3}\left(\frac{\ell}{\xi}\right)^2 m + \frac{3}{\pi}\upsilon\left(\frac{\ell}{\xi}\right)^3 m^2 - Q\xi\left(\frac{\ell_B}{\ell}\right)e^{-\kappa\ell} \tag{7}$$

$$\frac{nF_{tie}\left(\frac{\xi}{\sqrt[3]{n}}, \frac{m}{n}\right)}{k_BT} = n\ln\left(\frac{\xi^5 n^{-5/3}}{16\pi\ell^5}\right) + \frac{2\pi^2}{3}\left(\frac{\ell}{\xi}\right)^2 mn^{2/3} + \frac{3\upsilon}{\pi}\left(\frac{\ell}{\xi}\right)^3 m^2 - Qn^{2/3}\xi\left(\frac{\ell_B}{\ell}\right)e^{-\kappa\ell} \tag{8}$$

where k_B =1.38×10^{-23} J/K is the Boltzmann constant, ξ represents the size of crystal phase, υ is the excluded volume, ℓ is the segment length, ℓ_B is the Bjerrum length, Q is charge density, κ is the inverse Debye length, m is the initial molar number of crystal phase, and n is the molar number of crystal phase dispersed into CANs.

Here the ratio (E_{ratio}) of tail free energy and tie free energy is used as the Hamilton path [36]. This ratio can be obtained using the following equation,

$$E_{ratio} = \frac{F_{tail}(\xi, m)}{nF_{tie}\left(\frac{\xi}{\sqrt[3]{n}}, \frac{m}{n}\right)} \cong \frac{1}{\frac{2\pi^3\xi}{9m\upsilon\ell}n^{2/3}+1} = \frac{\ln\left(\frac{\xi}{4\ell}\right)+\frac{2\pi^2}{3}\left(\frac{\ell}{\xi}\right)^2 m+\frac{3}{\pi}\upsilon\left(\frac{\ell}{\xi}\right)^3 m^2-Q\xi\left(\frac{\ell_B}{\ell}\right)e^{-\kappa\ell}}{n\ln\left(\frac{\xi^5 n^{-5/3}}{16\pi\ell^5}\right)+\frac{2\pi^2}{3}\left(\frac{\ell}{\xi}\right)^2 mn^{2/3}+\frac{3}{\pi}\upsilon\left(\frac{\ell}{\xi}\right)^3 m^2-Qn^{2/3}\xi\left(\frac{\ell_B}{\ell}\right)e^{-\kappa\ell}} \quad (9)$$

Combining equations (1), (6) and (9), the constitutive stress-strain relationship is finally obtained for the semi-crystalline polymer,

$$\begin{cases} \sigma = \Phi_c \dfrac{E_c}{E_{ratio}}\varepsilon + \displaystyle\sum_{i=1}^{n}\Phi_{ai}E_{ai}\tau_i\dot{\varepsilon}\left[1-\exp\left(-\frac{\varepsilon}{\tau_i\dot{\varepsilon}}\right)\right] \\ E_a = \displaystyle\sum_{i=1}^{n}E_{ai} = 3\left[N+\frac{tN_{t0}\exp\left(-\frac{\gamma}{(1-k_{so}t)\Delta V}-\frac{E_{ab}}{RT}\right)}{\tau_0+\frac{l_0^2}{D_0}\exp\left(\frac{E_{as}-E_{ab}}{RT}\right)}\right]RT \\ E_{ratio} = \dfrac{1}{\frac{2\pi^3\xi}{9m\upsilon\ell}n^{2/3}+1} \end{cases} \quad (10)$$

Based on the equation (10), analytical results of the stresses of semi-crystalline epoxy as a function of the strain were obtained, and the data are plotted in Figure 5. During the calculations, the following parameters were used: ξ=45.2 nm [31], ℓ =1nm [31], γ=0.6 [39], D_0c=9.6×10^{-11} m^2/s [41], E_{as}=26.8×10^3 J/mol [18], Eab=1.22×10^3 J/mol [18], τ_0=0.023 s [18], ΔV=0.105, and k_{so}=3.98×10^{-5} s^{-1}. As shown in Figure 5(a), the obtained stress is increased from 73 MPa, 124 MPa, 227 MPa to 409 MPa, with an exponential increase in the fraction of crystal phase (Φ_c) from 2^{-4}, 2^{-3}, 2^{-2} to 2^{-1}, at the same strain of ε=0.1. These analytical results clearly indicate that the crystal phase

can increase the strength of semi-crystalline epoxy polymer, i.e., the strength is significantly increased with the fraction of crystal phase (Φ_c). This can be explained by the Hamiltonian graph theory [36]. With an increase in the fraction of crystal phase (Φ_c), which works as the vertex in the polymer network, the junction functionality between the vertex and side is increased. This results in the increase in both the cross-linking density and modulus, thus a much higher stress is achieved at the same strain.

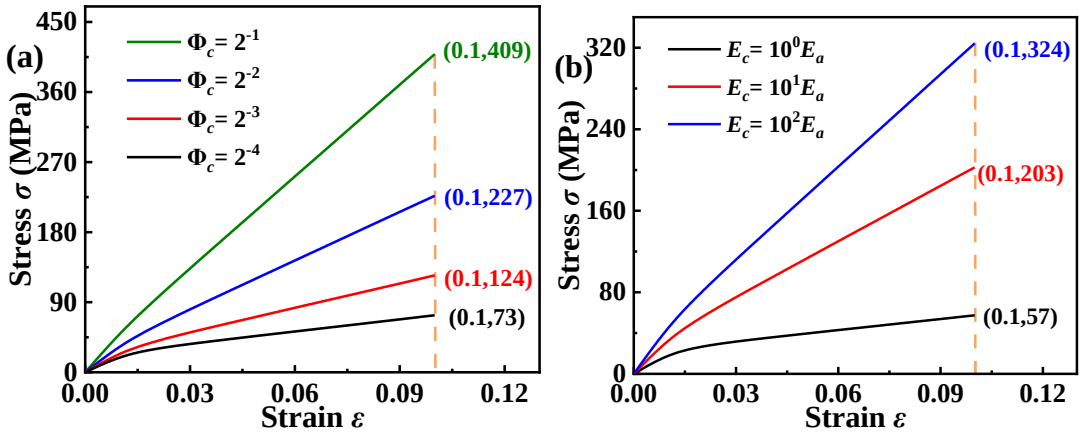

Figure 5. Effect of crystal phase on the constitutive stress-strain relationship. (a) Effect of fraction of crystal phase (Φ_c) on the constitutive stress-strain relationship. (b) Effect of moduli of crystal phases (E_c) on the constitutive stress-strain relationship.

On the other hand, effect of modulus of amorphous phase (*Ec*) on the constitutive stress-strain relationship was investigated based on the proposed model of equation (10), and the obtained results are plotted in Figure 5(b). Results show that the strengths are 57 MPa, 203 MPa and 324 MPa, for the semi-crystalline polymers with moduli of crystal phases of E_c=E_a, E_c=10E_a and E_c=10^2E_a, respectively, at the same strain of ε=0.1. These analytical results clearly indicate that the crystal phases are able to improve the strength of the semi-crystalline polymer, and the strength has been significantly increased with the modulus of crystal phases (*Ec*).

4. Experimental verification and finite element analysis

To verify the correctness of equation (10), tensile testing experiments of the epoxy specimens, i.e., amorphous epoxy, semi-crystalline epoxy, amorphous epoxy with BER and semi-crystalline epoxy with BER, were conducted, and the obtained results were compared with the analytical results based on the proposed model. All the values of parameters used in the calculations based on the equation (10) are listed in Table 1. The experimentally obtained stress-strain curves of all the specimens are plotted in Figure 6(a). The moduli of the epoxy specimens are gradually increased from 832 MPa (for amorphous epoxy), 926 MPa (for semi-crystalline epoxy), 1760 MPa (for amorphous epoxy with BERs) to 1889 MPa (semi-crystalline epoxy with BERs). This enhancement is mainly attributed to the coupling effect of crystalline structures and BER, both of which can increase the mechanical moduli of the semi-crystalline epoxy polymers. Furthermore, tensile fracture strains of the specimens were found to be 0.27 (for amorphous epoxy), 0.08 (for amorphous epoxy with BERs), 0.10 (for semi-crystalline epoxy) and 0.31 (for semi-crystalline epoxy with BERs), respectively. These experimental results clearly reveal that the crystal phase plays a negative effect on the fracture strain, and the BER plays a positive effect on the fracture strain. Whereas the coupling effect of crystal phase and BER enables the epoxy polymer having achieved an extremely high fracture strain. Owing to the coupling effect of crystal phase and BER, the fracture energies of epoxy specimens were found to be 5121 kJ/m^3 (for amorphous epoxy), 2035 kJ/m^3 (for amorphous epoxy with BERs), 2502 kJ/m^3 (for semi-crystalline epoxy) and 7470 kJ/m^3 (for semi-crystalline epoxy

with BERs), respectively, as shown in Figure 6(b).

Table 1. Parameters used in the equation (10)

	Epoxy	Epoxy with BERs	Semi-crystalline epoxy	Semi-crystalline epoxy with BERs
$\sum E_a$(MPa)	832	1760	887	3023
$\tau\dot{\varepsilon}$	0.02	0.09	5.01	0.07

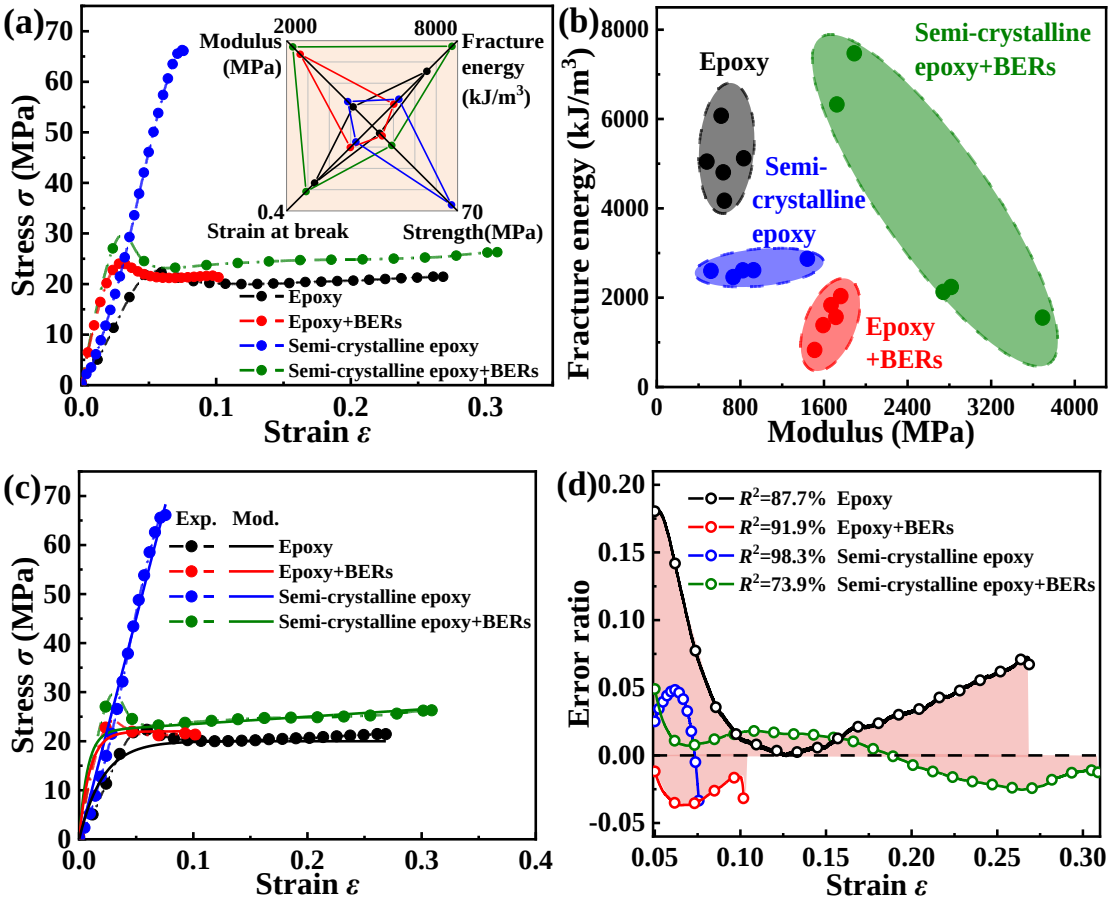

Figure 6. Analytical results from current model and experimental data of stress-strain curves of four types of epoxy specimens. (a) Experimental measurements of mechanical stress-strain curves. (b) Fracture energy as a function of modulus. (c) Comparison between analytical and experimental results of stress-strain curves. (d) Divergences of analytical and experimental results of stress.

Experimental data of the epoxy specimens were collected to verify the analytical results derived from the proposed model based on the equation (10). Levenberg-Marquardt optimization algorithm was adopted for all the calculation parameters, where Origin® software was used to carry out Levenberg-Marquardt optimizations

and fit the theoretical parameters based on the experimental data. All the parameters used in calculations are listed in Table 1. As shown in Figure 6(c), the analytical results agree well with the experimental data. Figure 6(d) shows that the correlation index R^2 between the analytical and experimental results are 87.9%, 91.9%, 98.9%and 73.9% for the amorphous epoxy, amorphous epoxy with BERs, semi-crystalline epoxy, and semi-crystalline epoxy with BERs, respectively, where the error ratio of stress is limited to 18%.

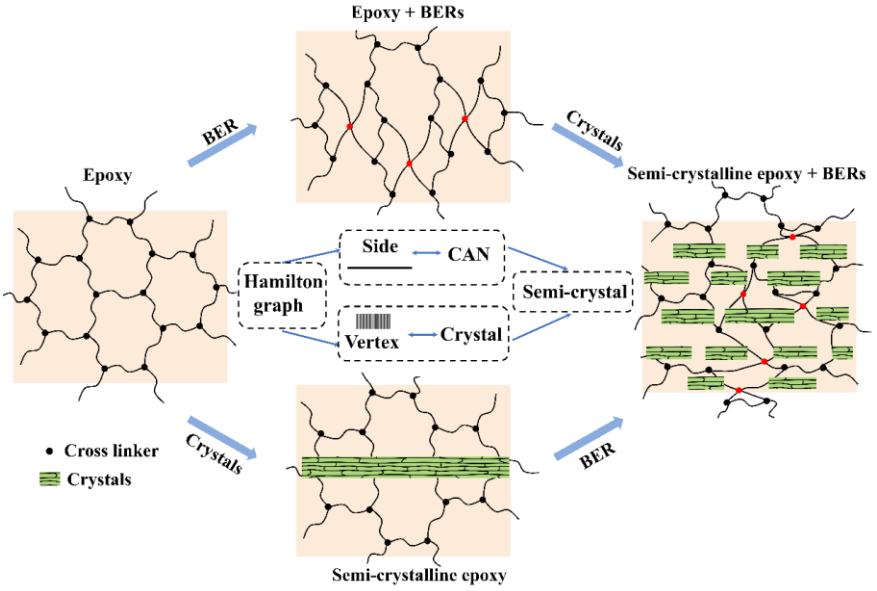

Figure 7. Schematic illustration of cooperative coupling of crystal phases and CANs using Hamiltonian graph model in semi-crystalline epoxy.

The working principles for the toughening mechanisms and cooperative effects of crystal phases and CANs are illustrated in Figure 7. Based on the Hamiltonian graph model, there is a cooperative coupling between crystal phase and CAN, and the crystalline phase is used as the vertex to increase the number of Hamiltonian paths. Meanwhile, the CAN improves homogeneous dispersion of the crystalline phase in the polymer network, thus resulting in an indirect increase in the number of

Hamiltonian paths. Furthermore, the crystalline phases with their higher fractions and moduli further enhance the stiffness and strength. Whereas the CANs enable the semi-crystalline epoxy with a good stretchability. Therefore, the toughening mechanism is originated from the cooperative coupling of both crystal phases and CANs, therefore the semi-crystalline epoxy shows a good toughening behavior.

FEA was used to study the effects of crystal fraction (Φ_c) and modulus of crystal phase (E_c) on the mechanical stress-strain behavior of the semi-crystalline epoxy. About 2000 solid elements of the 8-node hexahedron, C3D8R, were used to model the unit under a static simulation condition. Boundary conditions with fix constraints were applied to the nodes on one side and uniform displacements of loads were applied on the other side, as shown in Figure 8(a). Figure 8(b) shows that the maximum error under different sensitivity changes is 9.95%, and the calculated results are reliable regarding to the sensitivity of the element. In Figure 8(c), the mesh refinement degree is changed from 1k to 3k, and the position of the simulation calculation is more specific with the increase of the sensitivity.

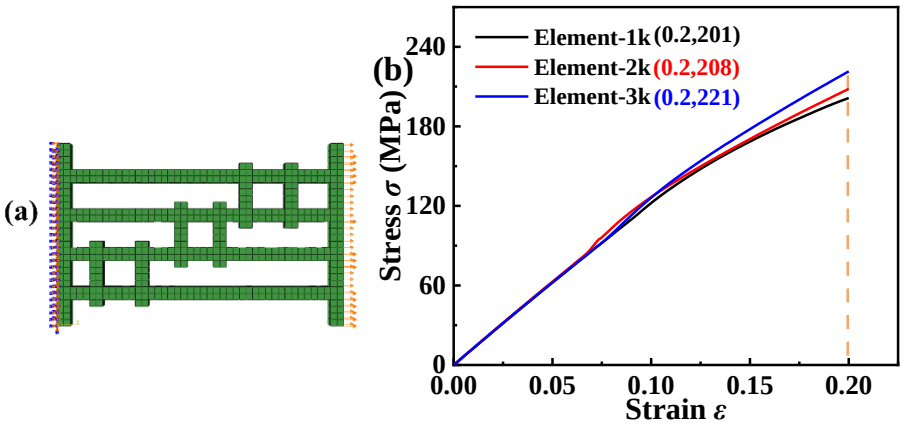

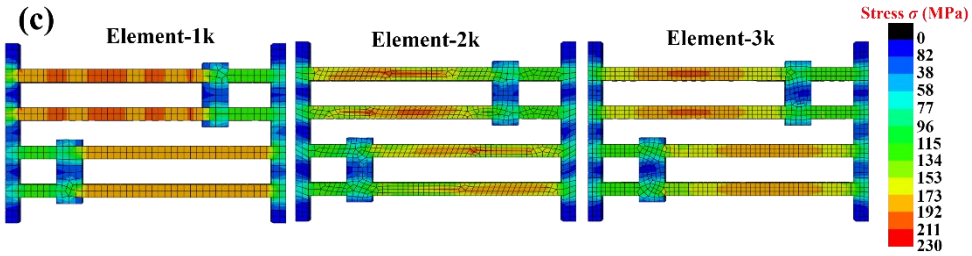

Figure 8. (a) Boundary conditions for FEA simulations. (b) Effect of different precision elements. (c) FEA simulations of effect of mesh sensitivity.

FEA diagrams in Figures 9(a) and 9(b) show that the obtained stresses of semi-crystalline epoxy specimens are increased from 171 MPa, 201 MPa to 274 MPa, when the crystal fractions (Φ_c) are increased from 2^{-4}, 2^{-3} to 2^{-2} at the same modulus of E_c=E_a. Furthermore, the dispersion of crystal phase plays a critical role to influence the mechanical behavior of the semi-crystalline epoxy with BERs. Results show that the stresses are increased from 178 MPa, 239 MPa to 298 MPa, in comparisons with that the epoxy specimens without dispersion of crystal phase, at the same crystal phase fraction (Φ_c) and modulus. The stress of the semi-crystalline epoxy without crystal phase (Φ_c=0) is 146 MPa, as shown in Figure 9(c). Whereas those values are 298 MPa, 340 MPa and 343 MPa, for the semi-crystalline polymers with moduli of crystal phases of E_c, $10^{-1}E_c$ and $10^{-2}E_c$, respectively. The simulation results clearly reveal that the mechanical properties of the epoxy polymers are significantly enhanced by the increase in crystal phase fraction (Φ_c) and modulus of crystal phase (E_c) in the semi-crystalline epoxy.

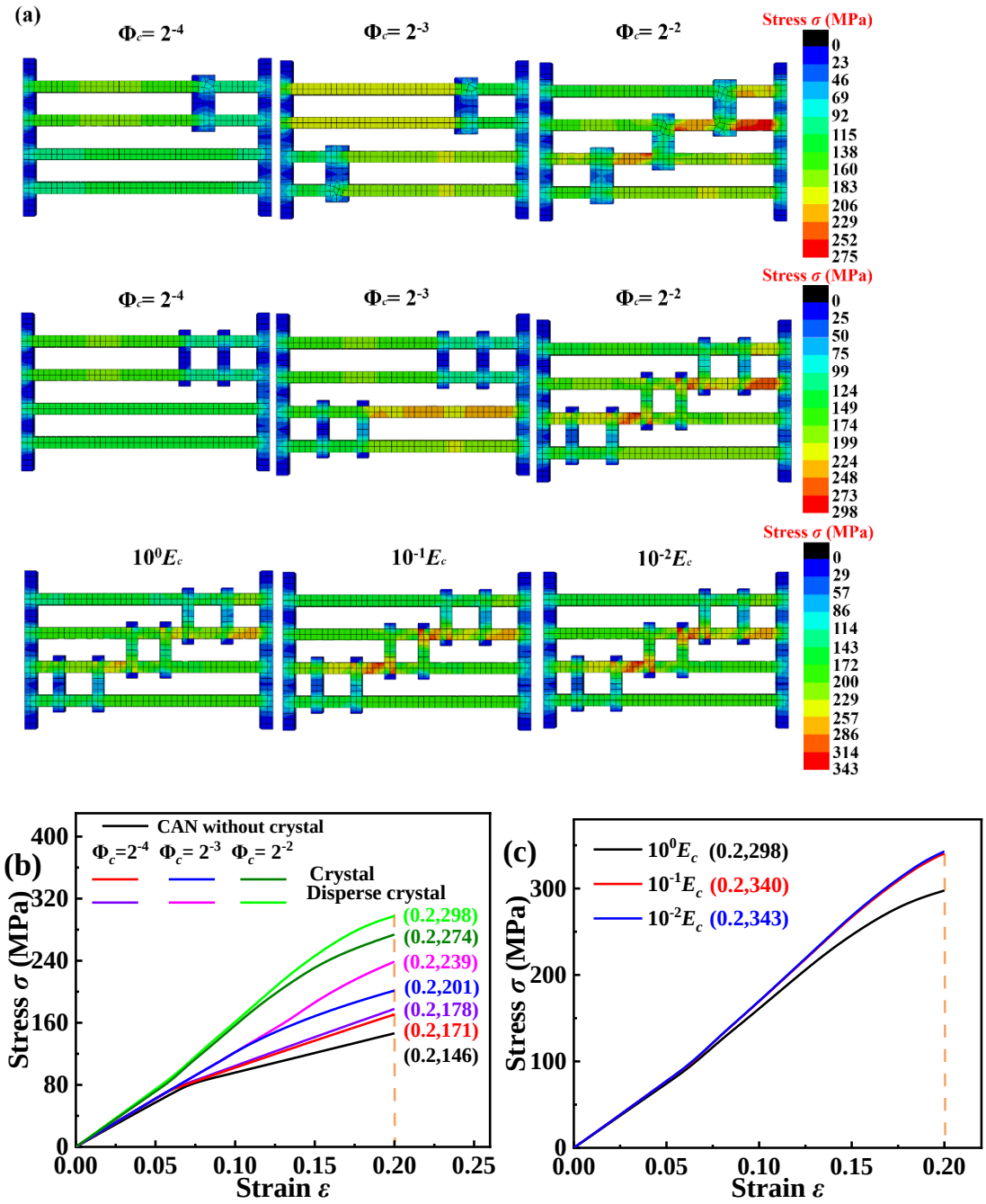

Figure 9. (a) FEA simulations of effect of crystal phases on the stress-strain in semi-crystalline epoxy. (b) Effect of fraction of crystal phases (Φ_c) on the stress-strain in semi-crystalline epoxy. (c) Effect of modulus of crystal phases (E_c) on the stress-strain in semi-crystalline epoxy.

5. Conclusion

A Hamilton graph model is established to investigate the toughening mechanism and cooperative coupling of crystal phases and CANs in the semi-crystalline epoxy. It

has been found that the crystal phases work as the vertexes to enhance the Hamilton paths for CANs, which improve the homogenous dispersions of the crystal phases and enhance the number of vertexes. A strong cooperative coupling of crystal phases and CANs has resulted in an effective toughening effect for the semi-crystalline epoxy. Furthermore, a free-energy equation is formulated to describe the effects of fraction and modulus of crystal phase on the mechanical behaviors of the semi-crystalline epoxy. Then the constitutive stress-strain relationship has been developed to identify the toughening mechanisms owing to the cooperative coupling, based on the Hamilton graph theory and extended Maxwell model. Finally, the proposed framework is verified using both the FEA simulations and experimental data of mechanical properties of a semi-crystalline epoxy. This newly proposed model provides a new insight into the Hamiltonian graph to explore the toughening mechanism of crystalline phases and CANs in the semi-crystalline thermoset epoxy. Our research results prove the effectiveness of a new technical methodology, which can be applied to enhance the fracture energy up to 46% and fracture strain up to 15%. This methodology can be applied to different crystalline systems, with the support from the finite element simulation, thermodynamic analysis and experimental data.

Acknowledgements

This work was financially supported by the National Natural Science Foundation of China (NSFC) under Grant No. 11725208 and 12172107, International Exchange Grant (IEC/NSFC/201078) through Royal Society UK and the NSFC.

References

[1] Khan A, Ahmed N, Rabnawaz M 2020 Covalent adaptable network and self-healing materials: current trends and future prospects in sustainability *Polymers-Basel* **12** 2027

[2] Xu X W, Ma S Q, Wang S, Wang B B, Feng H Z, Li P Y, Liu Y L, Yu Z, Zhu J 2022 Fast-reprocessing, postadjustable, self-healing covalent adaptable networks with schiff base and diels-alder adduct *Macromol. Rapid Commun.* **43** 2100777

[3] Zhang L Z, You Z W 2021 Dynamic oxime-urethane bonds, a versatile unit of high performance self-healing polymers for diverse applications *Chin. J. Polym. Sci.* **39** 1281-1291

[4] Van Lijsebetten F, Spiesschaert Y, Winne J M, Du Prez F E 2021 Reprocessing of covalent adaptable polyamide networks through internal catalysis and ring-size effects *J. Am. Chem. Soc.* **143** 15834-15844

[5] Zeng Y N, Liu S X, Xu X M, Chen Y, Zhang F A 2020 Fabrication and curing properties of o-cresol formaldehyde epoxy resin with reversible cross-links by dynamic boronic ester bonds *Polymer* **211** 123116

[6] Li P Z, Lan B, Zhang X T, Lei S Y, Yang Q, Gong P J, Park C B, Li G X 2022 Facile in situ construction of a covalent adaptable network polyester vitrimer with advanced performance in repairability, foamability and recyclability *Green Chem*. **24** 5490-5501

[7] Liguori A, Hakkarainen M 2022 Designed from biobased materials for recycling: imine-based covalent adaptable networks *Macromol. Rapid Commun.* **43** 2100816

[8] Abd-Elnaiem A M, Salman O S, Hakamy A, Hussein S I 2022 Mechanical characteristics and thermal stability of hybrid epoxy and acrylic polymer coating/nanoclay of various thicknesses *J. Inorg. Organomet. P.* **32** 2094-2102

[9] Kim K H, Kim M J, Kim J W, Lee K M, Kim H G, Lee Y-S 2019 Enhanced creep behavior of carbon black/epoxy composites with high dispersion stability by fluorination *Carbon Lett.* **29** 643-648

[10] Jones A R, Watkins C A, White S R, Sottos N R 2015 Self-healing thermoplastic-toughened epoxy *Polymer* **74** 254-261

[11] Paolillo S, Bose R K, Santana M H, Grande A M 2021 Intrinsic self-healing epoxies in polymer matrix composites (PMCs) for aerospace applications *Polymers-Basel* **13** 201

[12] Li Y H, Guo W J, Li W J, Liu X, Zhu H, Zhang J P, Liu X J, Wei L H, Sun A L 2020 Tuning hard phase towards synergistic improvement of toughness and self-healing ability of poly(urethane urea) by dual chain extenders and coordinative bonds *Chem. Eng. J.* **393** 124583

[13] Odarczenko M, Thakare D, Li W, Venkateswaran S P, Sottos N R, White S R 2020 Sunlight-activated self-healing polymer coatings *Adv. Eng. Mater.* **22** 1901223

[14] Casado J, Konuray O, Roig A, Fernández-Francos X, Ramis X 2022 3D printable

hybrid acrylate-epoxy dynamic networks *Eur. Polym. J.* **173** 111256

[15] He X, Lei Z P, Zhang W, Yu K 2019 Recyclable 3d printing of polyimine-based covalent adaptable network polymers *3d Print. Addit. Manuf.* **6** 31-39

[16] Yu K, Xie T, Leng J S, Ding Y F, Qi H J 2012 Mechanisms of multi-shape memory effects and associated energy release in shape memory polymers *Soft Matter* **8** 5687

[17] Yu K, Yang H, Dao B H, Shi Q, Yakacki C M 2017 Dissolution of covalent adaptable network polymers in organic solvent *J. Mech. Phys. Solids* **109** 78-94

[18] Shi X J, Luo C Q, Lu H B, Yu K 2021 Interfacial welding and reprocessing of engineering thermosets based on surface depolymerization *Surf. Interfaces* **26** 101368

[19] Xing Z Y, Shu D W, Lu H B, Fu Y-Q 2022 Untangling the mechanics of entanglements in slide-ring gels towards both super-deformability and toughness *Soft Matter* **18** 1302-1309

[20] Xing Z Y, Lu H B, Fu Y Q 2021 Local conservation law of rubber elasticity in hydrogel networks undergoing microphase separation and toughening *Polymer* **222** 123656

[21] Arumugam S, Kandasamy J, Sultan M T H, Shah A U M, Safri S N A 2021 Investigations on fatigue analysis and biomimetic mineralization of glass fiber/sisal fiber/chitosan reinforced hybrid polymer sandwich composites *J. Mater. Res. Technol.* **10** 512-525

[22] Ji B H, Gao H J 2004 Mechanical properties of nanostructure of biological

materials *J. Mech. Phys. Solids* **52** 1963-1990

[23] Liu B, Zhang L X, Gao H J 2006 Poisson ratio can play a crucial role in mechanical properties of biocomposites *Mech. Mater.* **38** 1128-1142

[24] Righetti M C, Aliotta L, Mallegni N, Gazzano M, Passaglia E, Cinelli P, Lazzeri A 2019 Constrained amorphous interphase and mechanical properties of poly(3-hydroxybutyrate-co-3-hydroxyvalerate) *Front Chem* **7** 790

[25] Righetti M C, Tombari E 2011 Crystalline, mobile amorphous and rigid amorphous fractions in poly(L-lactic acid) by TMDSC *Thermochim. Acta* **522** 118-127

[26] Wunderlich B 2005 Effect of decoupling of molecular segments, microscopic stress-transfer and confinement of the nanophases in semicrystalline polymers *Macromol. Rapid Commun.* **26** 1521-1531

[27] Gohari S, Mouloodi S, Mozafari F, Alebrahim R, Moslemi N, Burvill C, Albarody TMB 2021 A new analytical solution for elastic flexure of thick multi-layered composite hybrid plates resting on Winkler elastic foundation in air and water *Ocean Eng.* **235** 109372

[28] Gohari S, Sharifi S, Burvill C, Mouloodi S, Izadifar M, Thissen P 2019 Localized failure analysis of internally pressurized laminated ellipsoidal woven GFRP composite domes: Analytical, numerical, and experimental studies *Arch. Civ. Mech. Eng.* **19** 1235-1250

[29] Gohari S, Mozafari F, Moslemi N, Mouloodi S, Alebrahim R, Ahmed M, Abdi B, Sudin I, Burvill C 2022 Static and dynamic deformation response of smart

laminated composite plates induced by inclined piezoelectric actuators *J. Compos. Mater.* **56** 3269-3293

[30] Wang X D, Lu H B, Gorbacheva G, Hossain M, Fu Y Q 2021 Multi-modal commutative dynamics in semi-crystalline polymers undergoing multiple shape memory behavior *Smart Mater. Struct.* **30** 045003

[31] Jia D, Muthukumar M 2021 Electrostatically driven topological freezing of polymer diffusion at intermediate confinements *Phys. Rev. Lett.* **126** 057802

[32] Jaques N G, Barros J J P, dos Santos Silva I D, Popp M, Kolbe J, Wellen R M R 2021 Crossing over the curing and degradation of DGEBA/MTHPA/Eggshell to disclose the reactionary system *Compos. Part. B-Eng.* **224** 109181

[33] Liu C Z, Sun M M, Zhang B, Zhang X G, Li J H, Wang L, Xue G, Zhao M, Song C Y, Li Q L 2017 Preparation and properties of acetylene-terminated benzoxazine/epoxy copolymers *React. Funct. Polym.* **120** 98-103

[34] Morgan R J, O'Neal J E 1978 The durability of epoxies *Polym.-Plast. Technol. Eng.* **10** 49-116

[35] Carlborg C F, Vastesson A, Liu Y, van der Wijngaart W, Johansson M, Haraldsson T 2014 Functional off-stoichiometry thiol-ene-epoxy thermosets featuring temporally controlled curing stages via an UV/UV dual cure process *J. Polym. Sci. Pol. Chem.* **52** 2604-2615

[36] Chartrand G, Zhang P 2012 A first course in graph theory. New York: Dover Publications Inc Press

[37] Fried J R 2014 Polymer science and technology. United States of America:

Pearson Education Press

[38] Treloar L R G 1975 The physics of rubber elasticity. New York: Oxford University Press

[39] Macedo P B, Litovitz T A 1965 On the relative roles of free volume and activation energy in the viscosity of liquids *J. Chem. Phys.* **42** 245-256

[40] Stukalin E B, Cai L-H, Kumar N A, Leibler L, Rubinstein M 2013 Self-healing of unentangled polymer networks with reversible bonds *Macromolecules* **46** 7525-7541

[41] Chen S H, Chu B, Nossal R 1981 Scattering techniques applied to supramolecular and nonequilibrium systems. New York: Plenum Press